H. Cho
Graduate Student.

G. A. Kardomateas
Professor.
Mem. ASME.

C. S. Valle
Graduate Student.

School of Aerospace Engineering,
Georgia Institute of Technology,
Atlanta, GA 30332-0150

Elastodynamic Solution for the Thermal Shock Stresses in an Orthotropic Thick Cylindrical Shell

An elastodynamic solution for the thermal shock stresses in an orthotropic thick cylindrical shell is presented. The solution is achieved by the proper usage of integral transforms such as the finite Hankel transform and the Laplace transform. No restrictive assumptions on the shell thickness are placed. Results are presented for the well-formed wave propagation phenomenon of elastic stresses through the thickness of an orthotropic thick cylindrical shell. Thermal shock stresses become of significant magnitude due to stress wave propagation which is initiated at the boundaries by sudden thermal loading.

Introduction

In recent years, attention to thick composite shells has been continuously increased in several industrial areas. Thick composite cylindrical shells can be used in applications involving aerospace, offshore and submarine structures, pressure vessels, civil engineering structures, chemical pipes, and even automotive suspension components. These structures can be easily exposed to a variety of temperature fields in different environments. In high-temperature applications, thermal stresses, which are induced from the heat build up and cooling processes, may rise above the ultimate strength and lead to unexpected failures. Thus, the importance of thermal stresses in causing structural damage and changes in the functionality of the structure is well recognized whenever thermal environments are involved. Therefore, the capability to predict elastodynamic stresses induced by sudden thermal loading in composite structures is essential for the proper and safe design and the knowledge of its response during service in these severe thermal applications.

In the case of suddenly applied thermal loading, thermal deformation and the role of inertia become larger. Since the thermal stress changes very rapidly, the static analysis cannot capture its behavior. This dynamic thermoelastic stress response is significant and leads to the propagation of elastic stress waves in the solid.

Regarding related work, Sneddon (1951) introduced the finite Hankel transform to solve the heat conduction problems. The finite Hankel transform was successfully applied to the boundary value problem of heat conduction by Cinelli (1965) and later the usefulness of applications to dynamic problems for cylindrical and spherical shells was also studied (Cinelli, 1966).

The three-dimensional elasticity approach is the most powerful way to analyze the elastodynamic behavior when thick construction is involved. Elasticity approaches for orthotropic cylindrical shells have been used for static and dynamic stress analysis in several instances. Hyer and Cooper (1986) studied the static stresses and deformations induced by a circumferential temperature gradient in a composite tube. Kardomateas (1989, 1990) also used the elasticity approach to obtain the transient (but without the inertia term) thermal stresses in an orthotropic composite thick tube.

The thermal shock problem, which is a dynamic thermoelastic problem, was studied by Birman (1990) for a composite hollow cylinder based on the Donnell type of thin shell theory. Several other contributions using the elasticity approach to the thermal shock problem have been made, which are mostly related to an infinite elastic body with a spherical cavity (Sternberg and Chakravorty, 1959) and hollow spherical shells (Tsui and Kraus, 1965; Zaker, 1969). Another considerable work for the thermal shock stresses in a hollow sphere due to rapid uniform heating was performed by Hata (1991). The Ray theory was employed by taking the thermoelastic displacement potential for the thermoelastic equation and the displacement potential for the dynamic elasticity equation. The dynamic, thermoelastic response of thin cylindrical shells to suddenly applied and rotating thermal loadings was studied by McQuillen and Brull (1970). Sciuva and Carrera (1992) numerically investigated the elastodynamic behavior of relatively thick symmetrically laminated anisotropic circular shells as a plane-strain problem by the first-order shear deformation theory. Wang and Gong (1992) obtained the analytic solution using the finite Hankel transform and the Laplace transform for elastodynamic problems and presented the elastodynamic solution for a multilayered isotropic hollow cylinder. Wang (1993, 1995) dealt with the stress wave propagation problem in a two layered cylinder with initial interface pressure and investigated the thermal shock stresses caused by rapidly increasing uniform heating to an isotropic hollow cylinder as a plane-strain problem. But their studies were confined only to isotropic shell problems.

Even though several papers have been written in this area, the elastodynamic solution for a generally orthotropic cylindrical shell has not yet been reported. Thus, in this study, the finite Hankel transform and the Laplace transform are used to solve the uncoupled linear dynamic thermoelasticity problem for an orthotropic cylindrical shell. The advantage of this method is the ability to provide a closed-form solution which is applicable to a generally orthotropic cylinder of arbitrary thickness. This requires the use of the Bessel functions of the first and/or the second kind of arbitrary order due to the orthotropy of material constants.

Formulation

Consider a hollow cylinder subjected to a specific temperature environment with or without external pressure. The inner

Contributed by the Applied Mechanics Division of THE AMERICAN SOCIETY OF MECHANICAL ENGINEERS for publication in the ASME JOURNAL OF APPLIED MECHANICS.

Discussion on the paper should be addressed to the Technical Editor, Professor Lewis T. Wheeler, Department of Mechanical Engineering, University of Houston, Houston, TX 77204-4792, and will be accepted until four months after final publication of the paper itself in the ASME JOURNAL OF APPLIED MECHANICS.

Manuscript received by the ASME Applied Mechanics Division, Oct. 15, 1996; final revision, May 12, 1997. Associate Technical Editor: U. K. Kinra.

and outer radii are denoted by r_1 and r_2, respectively. We denote by r the radial, θ the circumferential, and z the axial coordinate. The hollow cylinder is assumed to have zero initial temperature, but at $t > 0^+$, the shell is kept at a constant temperature through the thickness. Since there is only radial dependence of the temperature field, the hoop displacements are zero and the stresses and strains are independent of θ. Thus the thermoelastic stress-strain relations for the orthotropic body are

$$\begin{bmatrix} \sigma_{rr} \\ \sigma_{\theta\theta} \\ \sigma_{zz} \\ \tau_{\theta z} \\ \tau_{rz} \\ \tau_{r\theta} \end{bmatrix} = \begin{bmatrix} c_{11} & c_{12} & c_{13} & 0 & 0 & 0 \\ c_{12} & c_{22} & c_{23} & 0 & 0 & 0 \\ c_{13} & c_{23} & c_{33} & 0 & 0 & 0 \\ 0 & 0 & 0 & c_{44} & 0 & 0 \\ 0 & 0 & 0 & 0 & c_{55} & 0 \\ 0 & 0 & 0 & 0 & 0 & c_{66} \end{bmatrix} \begin{bmatrix} \epsilon_{rr} - \alpha_r \Delta T \\ \epsilon_{\theta\theta} - \alpha_\theta \Delta T \\ \epsilon_{zz} - \alpha_z \Delta T \\ \gamma_{\theta z} \\ \gamma_{rz} \\ \gamma_{r\theta} \end{bmatrix}, \tag{1}$$

where c_{ij} are the elastic constants and α_i are the thermal expansion coefficients (1, 2, and 3 represent r, θ, and z directions, respectively). The geometry of shell is assumed to be axisymmetric. Since the temperature doesn't depend on the axial coordinate, it is assumed that the stresses are independent of z. In addition to the constitutive Eq. (1), the elastic response of the cylinder must satisfy the dynamic equilibrium equations. Only one equilibrium equation remains, since $\tau_{\theta z} = \tau_{rz} = \tau_{r\theta} = 0$.

$$\frac{\partial \sigma_{rr}}{\partial r} + \frac{\sigma_{rr} - \sigma_{\theta\theta}}{r} = \rho \frac{\partial^2 u_r}{\partial t^2}, \tag{2}$$

where ρ denotes the density of material.

For the problem without the thermal effects, the expressions for the displacement field were derived by Lehknitskii (1963).

$$u_r = U(r, t) + z(w_y \cos\theta - w_x \sin\theta) + u_0 \cos\theta + v_0 \sin\theta, \tag{3}$$

$$u_\theta = -z(w_y \sin\theta + w_x \cos\theta) + w_z r - u_0 \sin\theta + v_0 \cos\theta, \tag{4}$$

$$u_z = zf(t) - r(w_y \cos\theta - w_x \sin\theta) + w_0, \tag{5}$$

where the function $U(r, t)$ represents the radial displacement accompanied by deformation. The constants u_0, v_0, w_0, w_x, w_y, and w_z denote the rigid-body translation and rotation along the x, y, and z directions in the Cartesian coordinate system, respectively. The time-dependent parameter $f(t)$ is determined from the boundary conditions.

The strains are expressed in terms of the displacements as follows:

$$\epsilon_{rr} = \frac{\partial U(r, t)}{\partial r}, \quad \epsilon_{\theta\theta} = \frac{U(r, t)}{r}, \quad \epsilon_{zz} = f(t), \quad \gamma_{\theta z} = \gamma_{rz} = \gamma_{r\theta} = 0. \tag{6}$$

Substituting (1) and (6) into the equilibrium Eq. (2) gives the following equation of dynamic thermoelasticity for the radial displacement $U(r, t)$:

$$c_{11}\left[\frac{\partial^2 U(r, t)}{\partial r^2} + \frac{1}{r}\frac{\partial U(r, t)}{\partial r}\right] - \frac{c_{22}}{r^2} U(r, t) = q_1 \frac{\partial T(r, t)}{\partial r} + q_2 \frac{T(r, t)}{r} + (c_{23} - c_{13}) \frac{f(t)}{r} + \rho \frac{\partial^2 U(r, t)}{\partial t^2}, \tag{7}$$

where, the q_i constants are given by

$$q_1 = c_{11}\alpha_r + c_{12}\alpha_\theta + c_{13}\alpha_z, \tag{8}$$

$$q_2 = (c_{11} - c_{12})\alpha_r + (c_{12} - c_{22})\alpha_\theta + (c_{13} - c_{23})\alpha_z, \tag{9}$$

and the initial conditions, as well as the boundary conditions due to the absence of external tractions, $\sigma_{rr}(r_i, t) = 0$, $i = 1, 2$, are

$$U(r, 0) = 0, \quad \frac{\partial U(r, 0)}{\partial t} = 0, \tag{10}$$

$$c_{11}\frac{\partial U(r_i, t)}{\partial r} + c_{12}\frac{U(r_i, t)}{r_i} + c_{13}f(t) - q_1 T(r_i, t) = 0, \quad i = 1, 2. \tag{11}$$

The axial force $P_z(t)$ is given by

$$P_z(t) = \int_{r_1}^{r_2} \sigma_{zz}(r, t) 2\pi r dr = \int_{r_1}^{r_2} \left[c_{13}\frac{\partial U(r, t)}{\partial r} + c_{23}\frac{U(r, t)}{r} + c_{33}f(t) - q_3 T(r, t)\right] 2\pi r dr, \tag{12}$$

where $q_3 = c_{13}\alpha_r + c_{23}\alpha_\theta + c_{33}\alpha_z$.

Consider now the thermoelastic equation of the present problem without the inertia term, which is described by the following inhomogeneous ordinary differential equation of second order in terms of the radial displacement $U_t(r, t)$:

$$c_{11}\left[\frac{\partial^2 U_t(r, t)}{\partial r^2} + \frac{1}{r}\frac{\partial U_t(r, t)}{\partial r}\right] - \frac{c_{22}}{r^2} U_t(r, t) = q_1 \frac{\partial T(r, t)}{\partial r} + q_2 \frac{T(r, t)}{r} + (c_{23} - c_{13}) \frac{f(t)}{r}. \tag{13}$$

Notice the absence of the dynamic term (last term in (7)). The associated initial conditions and boundary conditions are given as in (10) and (11) with U_t substituted in place of U. The axial force, $P_{z_t}(t)$, is also given by the same relation as in (12) with U_t substituted in place of U.

It is assumed that the general solution of the governing equation of linear dynamic thermoelasticity (7) can be separated into two parts, by the principle of superposition, namely,

$$U(r, t) = U_t(r, t) + U_d(r, t), \tag{14}$$

where $U_t(r, t)$ represents the thermoelastic radial displacement without the inertia term and $U_d(r, t)$ denotes the dynamic radial displacement.

As a particular case for the presented formulation, the temperature distribution which can be arbitrarily selected can be assumed as

$$T(r, t) = T_0 H(t) = \begin{cases} 0, & t < 0 \\ T_0, & t \geq 0^+ \end{cases}. \tag{15}$$

The function $f(t)$ is set in the same form, as

$$f(t) = f_0 H(t) = \begin{cases} 0, & t < 0 \\ f_0, & t \geq 0^+ \end{cases}, \tag{16}$$

where $H(t)$ is defined as the Heaviside step function. The general solution $U_t(r, t)$ of the inhomogeneous differential Eq. (13) is given by

$$U_t(r, t) = G_{10}r^{\lambda_1} + G_{20}r^{\lambda_2} + \frac{c_{23} - c_{13}}{c_{11} - c_{22}} f_0 r + U_t^*(r, t) \quad \text{for} \quad c_{11} \neq c_{22}, \quad (17)$$

or

$$U_t(r, t) = G_{10}r + G_{20}\frac{1}{r} + \frac{c_{23} - c_{13}}{2c_{11}} f_0 r \ln r + U_t^*(r, t) \quad \text{for} \quad c_{11} = c_{22}, \quad (18)$$

where $\lambda_{1,2} = \sqrt{c_{22}/c_{11}}$ and $U_t^*(r, t)$ is a particular solution, obtained as

$$U_t^*(r, t) = \begin{cases} T_0 q_2 r/(c_{11} - c_{22}) & \text{for} \quad c_{11} \neq c_{22}, \ t \geq 0^+ \\ T_0 q_2 r \ln r/(2c_{11}) & \text{for} \quad c_{11} = c_{22}, \ t \geq 0^+ \end{cases} \quad (19)$$

Using (7) with the associated initial and boundary conditions and the above definition, the following equation for the dynamic elasticity part in terms of displacement is obtained:

$$c_{11}\left[\frac{\partial^2 U_d(r, t)}{\partial r^2} + \frac{1}{r}\frac{\partial U_d(r, t)}{\partial r}\right] - \frac{c_{22}}{r^2} U_d(r, t) = \rho\left(\frac{\partial^2 U_t(r, t)}{\partial t^2} + \frac{\partial^2 U_d(r, t)}{\partial t^2}\right), \quad (20)$$

with the initial conditions

$$U_d(r, 0) = 0, \quad \frac{\partial U_d(r, 0)}{\partial t} = 0. \quad (21)$$

The boundary conditions for the traction-free surfaces of the cylinder and the axial force at the ends are given from (11) as follows:

$$c_{11}\frac{\partial U_d(r_i, t)}{\partial r} + c_{12}\frac{U_d(r_i, t)}{r_i} = 0, \quad i = 1, 2. \quad (22)$$

Moreover, the axial force condition is given from (12):

$$\int_{r_1}^{r_2}\left[c_{12}\frac{\partial U_d(r, t)}{\partial r} + c_{23}\frac{U_d(r, t)}{r}\right]2\pi r dr = 0, \quad (23)$$

where $r_i = r_1$, or r_2. The dynamic elasticity Eq. (20) is given in the form

$$\frac{\partial^2 U_d(r, t)}{\partial r^2} + \frac{1}{r}\frac{\partial U_d(r, t)}{\partial r} - \frac{\nu^2}{r^2} U_d(r, t) = \frac{1}{\bar{c}^2}\left(\frac{\partial^2 U_t(r, t)}{\partial t^2} + \frac{\partial^2 U_d(r, t)}{\partial t^2}\right), \quad (24)$$

where the parameter $\nu = \sqrt{c_{22}/c_{11}}$. Therefore $\nu = \lambda_1$ and the wave speed in the radial direction is denoted by $\bar{c} = \sqrt{c_{11}/\rho}$.

At this stage, in order to develop the procedure for solving the dynamic elasticity Eq. (24), let the solution be $U_{d_h}(r, t) = g(r)e^{-i\omega t}$, where ω is the natural frequency. Substituting $U_{d_h}(r, t)$ into (24), after assuming $U_t(r, t) = 0$ and setting $\xi = \omega/\bar{c}$, gives a standard Bessel equation as follows:

$$\frac{d^2 g(r)}{dr^2} + \frac{1}{r}\frac{dg(r)}{dr} + \left(\xi^2 - \frac{\nu^2}{r^2}\right)g(r) = 0, \quad (25)$$

with the Cauchy boundary conditions

$$\frac{dg(r_i)}{dr} + h_i g(r_i) = 0, \quad i = 1, 2, \quad (26)$$

where the constants are defined by

$$h_1 = \frac{c_{12}}{r_1 c_{11}}, \quad h_2 = \frac{c_{12}}{r_2 c_{11}}. \quad (27)$$

The general solution of the Bessel equation of arbitrary order ν is obtained by

$$g(r) = AJ_\nu(\xi r) + BY_\nu(\xi r), \quad (28)$$

where $J_\nu(x)$ is the Bessel function of the first kind of order ν and $Y_\nu(x)$ is the Bessel function of the second kind of order ν defined as

$$Y_\nu(\xi r) = \frac{J_\nu(\xi r)\cos \pi\nu - J_{-\nu}(\xi r)}{\sin \pi\nu}. \quad (29)$$

But when the order ν is an integer, the function $Y_n(z)$ should be taken by the limit definition

$$Y_n(z) = \lim_{\nu \to n} Y_\nu(z).$$

The definitions of $J_\nu(\xi r)$ and $J_{-\nu}(\xi r)$ are described in Appendix A. By using the boundary conditions, the general solution $g(r)$ of the Bessel equation can be written as the eigenfunction series

$$g(r) = \sum_i A_i D_\nu(\xi_i r), \quad i = 1, 2, \ldots, \infty, \quad (30)$$

where A_i are constants, the eigenfunction

$$D_\nu(\xi_i r) = J_\nu(\xi_i r)Y_a - Y_\nu(\xi_i r)J_a,$$

and ξ_i is a positive root of the transcendental equation:

$$J_a Y_b - J_b Y_a = 0, \quad (31)$$

where the parameters are defined as

$$J_a = \xi_i J_\nu'(\xi_i r_1) + h_1 J_\nu(\xi_i r_1), \quad J_b = \xi_i J_\nu'(\xi_i r_2) + h_2 J_\nu(\xi_i r_2),$$
$$Y_a = \xi_i Y_\nu'(\xi_i r_1) + h_1 Y_\nu(\xi_i r_1),$$
$$Y_b = \xi_i Y_\nu'(\xi_i r_2) + h_2 Y_\nu(\xi_i r_2). \quad (32)$$

After multiplying (30) by $D_\nu(\xi_i r)$ and r, and integrating in the finite range, we can find the constants A_i by using the orthogonality condition

$$A_i = \int_{r_1}^{r_2} r g(r) D_\nu(\xi_i r) dr \Big/ \int_{r_1}^{r_2} r[D_\nu(\xi_i r)]^2 dr. \quad (33)$$

In order to get the general solution of the Bessel equation, we use the finite Hankel transform of $g(r)$, denoted by $\hat{g}(\xi_i)$, defined by

$$\hat{g}(\xi_i) = \int_{r_1}^{r_2} r g(r) D_\nu(\xi_i r) dr. \quad (34)$$

Then the inverse of the finite Hankel transformation is given in the form

$$g(r) = \sum_i \frac{\hat{g}(\xi_i) D_\nu(\xi_i r)}{N(\xi_i)}, \tag{35}$$

where the normalizing factor $N(\xi_i) = \int_{r_1}^{r_2} r[D_\nu(\xi_i r)]^2 dr$ which is always positive. Therefore, setting $U_d(r, t)$ in place of $g(r)$, the radial displacement due to the dynamic elasticity contribution can be expressed as

$$U_d(r, t) = \sum_i \frac{\hat{u}_d(\xi_i, t) D_\nu(\xi_i r)}{N(\xi_i)}, \tag{36}$$

where the summation is taken over all the positive roots of the transcendental equation (31). The finite Hankel transform for the dynamic displacement is now written by

$$\hat{u}_d(\xi_i, t) = \int_{r_1}^{r_2} r U_d(r, t) D_\nu(\xi_i r) dr. \tag{37}$$

Taking the finite Hankel transform of the inhomogeneous Eq. (24) over r_1 and r_2, and using (31), the transformed equation results in

$$\frac{2J_a}{\pi J_b}\left[\frac{\partial U_d(r_2, t)}{\partial r} + h_2 U_d(r_2, t)\right] - \frac{2}{\pi}\left[\frac{\partial U_d(r_1, t)}{\partial r} + h_1 U_d(r_1, t)\right] - \xi_i^2 \hat{u}_d(\xi_i, t) = \frac{1}{\bar{c}^2}\left(\frac{\partial^2 \hat{u}_d(\xi_i, t)}{\partial t^2} + \frac{\partial^2 \hat{u}_t(\xi_i, t)}{\partial t^2}\right). \tag{38}$$

Since $U_d(r, t)$ satisfies the homogeneous boundary conditions (22) at each surface, the first two terms of the left-hand side of (38) should vanish. Thus the transformed equation becomes

$$-\xi_i^2 \hat{u}_d(\xi_i, t) = \frac{1}{\bar{c}^2}\left(\frac{\partial^2 \hat{u}_d(\xi_i, t)}{\partial t^2} + \frac{\partial^2 \hat{u}_t(\xi_i, t)}{\partial t^2}\right). \tag{39}$$

Using the Laplace transform, denoted by $\hat{u}_d^{\,L}$, with the zero initial conditions, the above equation can be transformed as

$$-\xi_i^2 \hat{u}_d^{\,L}(\xi_i, s) = \frac{s^2}{\bar{c}^2}[\hat{u}_d^{\,L}(\xi_i, s) + \hat{u}_t^{\,L}(\xi_i, s)]. \tag{40}$$

For convenience, the above equation can be written in the form

$$\hat{u}_d^{\,L}(\xi_i, s) = -\hat{u}_t^{\,L}(\xi_i, s) + \frac{\bar{c}^2 \xi_i^2}{\bar{c}^2 \xi_i^2 + s^2} \hat{u}_t^{\,L}(\xi_i, s). \tag{41}$$

By using the inverse Laplace transform, the following Hankel transformed dynamic displacement as a function of time is obtained from the previous equation

$$\hat{u}_d(\xi_i, t) = -\hat{u}_t(\xi_i, t) + \bar{c}\xi_i \sin \bar{c}\xi_i t * \hat{u}_t(\xi_i, t). \tag{42}$$

Since $U_t(r, t)$ is already known, the finite Hankel transform of $U_t(r, t)$, denoted by $\hat{u}_t(\xi_i, t)$, can be defined as follows:

$$\hat{u}_t(\xi_i, t) = \int_{r_1}^{r_2} r U_t(r, t) D_\nu(\xi_i r) dr. \tag{43}$$

Then, by using (17), the finite Hankel transform of the thermally induced displacement is described, for $c_{11} \neq c_{22}$, by

$$\hat{u}_t(\xi_i, t) = G_{10} I_1(\xi_i) + G_{20} I_2(\xi_i) + \frac{c_{23} - c_{13}}{c_{11} - c_{22}} f_0 I_3(\xi_i) + \hat{u}_t^*(\xi_i, t), \tag{44}$$

and, by using (18), for $c_{11} = c_{22}$,

$$\hat{u}_t(\xi_i, t) = G_{10} I_1(\xi_i) + G_{20} I_2(\xi_i) + \frac{c_{23} - c_{13}}{2c_{11}} f_0 I_3'(\xi_i) + \hat{u}_t^*(\xi_i, t). \tag{45}$$

Notice that the I_i's are the finite Hankel transforms, defined as

$$I_1(\xi_i) = \int_{r_1}^{r_2} r^{\nu+1} D_\nu(\xi_i r) dr,$$

$$I_2(\xi_i) = \int_{r_1}^{r_2} r^{-\nu+1} D_\nu(\xi_i r) dr. \tag{46}$$

These transforms can be analytically calculated from the recurrence formulas,

$$\frac{d}{dz}\{z^\nu J_\nu(z)\} = z^\nu J_{\nu-1}(z),$$

$$\frac{d}{dz}\{z^{-\nu} J_\nu(z)\} = -z^{-\nu} J_{\nu+1}(z), \tag{47}$$

regardless of the range of arguments. Thus the finite Hankel transforms $I_1(\xi_i)$ and $I_2(\xi_i)$ can be easily carried out analytically as given in Appendix B. Here the finite Hankel transform for $U_t^*(r, t)$ is given as

$$\hat{u}_t^*(\xi_i, t) = H\{U_t^*(r, t)\} = \int_{r_1}^{r_2} r U_t^*(r, t) D_\nu(\xi_i r) dr. \tag{48}$$

The finite Hankel transform of the above expression, using the earlier definition, becomes, for $c_{11} \neq c_{22}$,

$$\hat{u}_t^*(\xi_i) = \frac{T_0 q_2}{c_{11} - c_{22}} I_3(\xi_i), \tag{49}$$

and, for $c_{11} = c_{22}$,

$$\hat{u}_t^*(\xi_i) = \frac{T_0 q_2}{2c_{11}} I_3'(\xi_i), \tag{50}$$

where q_2 becomes zero for the isotropic case, for which $\alpha_r = \alpha_\theta$ and $c_{11} = c_{22}$. In the previous expression, I_3 and I_3' are the finite Hankel transforms of the functions r and $r \ln r$, described by

$$I_3(\xi_i) = \int_{r_1}^{r_2} r^2 D_\nu(\xi_i r) dr \quad \text{for} \quad c_{11} \neq c_{22}, \tag{51}$$

$$I_3'(\xi_i) = \int_{r_1}^{r_2} r^2 \ln r D_\nu(\xi_i r) dr \quad \text{for} \quad c_{11} = c_{22}. \tag{52}$$

The integration given by Eqs. (52) and (51) can be performed in closed form with the recurrence formulas available, only if the argument is in the small arguments domain and the definition

of series expansions for Bessel functions is used. The closed-form integration cannot be obtained in the large argument region for Eqs. (51) and (52). In this case, numerical integration should be used. Therefore, the Bessel functions for integration need to be computed in the two regions. One is for small arguments, the other is for large arguments. For the large arguments of the Bessel functions, the Hankel asymptotic expansions are always numerically integrated regardless of the order of Bessel functions because the closed form of integration cannot be obtained due to the complexity of the asymptotic definition of Bessel functions in this range. It can be noted that the numerical Hankel transform is always possible for any arbitrary analytical functions if the appropriate scheme of numerical integration is used. The Bessel functions of the first kind of order ν for small and large arguments used in this work are defined in Appendix A. Further details on the numerical finite Hankel transform will be mentioned in the next section.

Combining all these expressions, the finite Hankel transform of the dynamic displacement part is obtained by

$$\widehat{u}_d(\xi_i, t) = -\widehat{u}_t(\xi_i, t) + \bar{c}\xi_i \sin \bar{c}\xi_i t * \widehat{u}_t(\xi_i, t). \quad (53)$$

Thus, the convolution integral $I_0(t) = \int_0^t \widehat{u}_t(\xi_i, \tau) \sin \bar{c}\xi_i(t - \tau)d\tau$ is used and gives

$$\widehat{u}_d(\xi_i, t) = -\widehat{u}_t(\xi_i) \cos \bar{c}\xi_i t. \quad (54)$$

Substituting $\widehat{u}_d(\xi_i, t)$ into the inverse formula (36), the general solution of the dynamic part of the equation of motion is obtained by

$$U_d(r, t) = \sum_i \frac{D_\nu(\xi_i r)}{N(\xi_i)} [-\widehat{u}_t(\xi_i) \cos \bar{c}\xi_i t]. \quad (55)$$

Therefore, the general solution for the elastodynamic radial displacements due to thermal shock in an orthotropic thick cylindrical shell is found to be

$$U(r, t) = G_{10} r^{\lambda_1} + G_{20} r^{\lambda_2} + \left(\frac{c_{23} - c_{13}}{c_{11} - c_{22}} f_0 + \frac{T_0 q_2}{c_{11} - c_{22}} \right) r + \sum_i \frac{D_\nu(\xi_i r)}{N(\xi_i)} [-\widehat{u}_t(\xi_i) \cos \bar{c}\xi_i t]. \quad (56)$$

After obtaining the displacement (19) and its finite Hankel transform (49)–(50), the total displacement field (56) can be obtained. Therefore the elastodynamic thermal shock stresses in each direction can be determined from the relations (1) and (6) when $c_{11} \neq c_{22}$. The radial stress is

$$\begin{aligned}\sigma_{rr}(r, t) &= c_{11} \frac{\partial U(r, t)}{\partial r} + c_{12} \frac{U(r, t)}{r} + c_{13} f(t) - q_1 T(r, t) \\ &= G_{10}(c_{11}\lambda_1 + c_{12}) r_i^{\lambda_1 - 1} + G_{20}(c_{11}\lambda_2 + c_{12}) r_i^{\lambda_2 - 1} \\ &\quad + f_0 \left[c_{13} + \frac{c_{23} - c_{13}}{c_{11} - c_{22}} (c_{11} + c_{12}) \right] \\ &\quad - T_0 \left[q_1 - q_2 \frac{(c_{11} + c_{12})}{c_{11} - c_{22}} \right] \\ &\quad + \sum_i \frac{[-\widehat{u}_t(\xi_i) \cos \bar{c}\xi_i t]}{N(\xi_i)} \\ &\quad \times \left[c_{11} \frac{\partial D_\nu(\xi_i r)}{\partial r} + \frac{c_{12}}{r} D_\nu(\xi_i r) \right], \quad (57)\end{aligned}$$

the hoop stress is given by

$$\begin{aligned}\sigma_{\theta\theta}(r, t) &= c_{12} \frac{\partial U(r, t)}{\partial r} + c_{22} \frac{U(r, t)}{r} + c_{23} f(t) - q_{\alpha 2} T(r, t) \\ &= G_{10}(c_{12}\lambda_1 + c_{22}) r_i^{\lambda_1 - 1} + G_{20}(c_{12}\lambda_2 + c_{22}) r_i^{\lambda_2 - 1} \\ &\quad + f_0 \left[c_{23} + \frac{c_{23} - c_{13}}{c_{11} - c_{22}} (c_{12} + c_{22}) \right] \\ &\quad - T_0 \left[q_{\alpha 2} - q_2 \frac{(c_{12} + c_{22})}{c_{11} - c_{22}} \right] \\ &\quad + \sum_i \frac{[-\widehat{u}_t(\xi_i) \cos \bar{c}\xi_i t]}{N(\xi_i)} \\ &\quad \times \left[c_{12} \frac{\partial D_\nu(\xi_i r)}{\partial r} + \frac{c_{22}}{r} D_\nu(\xi_i r) \right], \quad (58)\end{aligned}$$

and the axial stress is given by

$$\begin{aligned}\sigma_{zz}(r, t) &= c_{13} \frac{\partial U(r, t)}{\partial r} + c_{23} \frac{U(r, t)}{r} + c_{33} f(t) - q_3 T(r, t) \\ &= G_{10}(c_{13}\lambda_1 + c_{23}) r_i^{\lambda_1 - 1} + G_{20}(c_{13}\lambda_2 + c_{23}) r_i^{\lambda_2 - 1} \\ &\quad + f_0 \left(c_{33} + \frac{(c_{23}^2 - c_{13}^2)}{(c_{11} - c_{22})} \right) \\ &\quad - T_0 \left[q_3 - q_2 \frac{(c_{13} + c_{23})}{(c_{11} - c_{22})} \right] \\ &\quad + \sum_i \frac{[-\widehat{u}_t(\xi_i) \cos \bar{c}\xi_i t]}{N(\xi_i)} \\ &\quad \times \left[c_{13} \frac{\partial D_\nu(\xi_i r)}{\partial r} + \frac{c_{23}}{r} D_\nu(\xi_i r) \right], \quad (59)\end{aligned}$$

where $q_{\alpha 2} = c_{12}\alpha_r + c_{22}\alpha_\theta + c_{23}\alpha_z$.

At this stage the unknown coefficients are found from the boundary conditions available. We have assumed that no external tractions exist. Then the conditions in the contour bounding the cross section (at r_1 and r_2) can be written in the following form:

$$\sigma_{rr}(r_i, t) = \tau_{r\theta}(r_i, t) = \tau_{rz}(r_i, t) = 0, \quad i = 1, 2. \quad (60)$$

Only a condition for the stress σ_{rr} is not satisfied identically and this is written as Eq. (57). By (60), the following linear equations in unknown constants G_{10}, G_{20}, and f_0 are obtained:

$$G_{10}(c_{11}\lambda_1 + c_{12}) r_i^{\lambda_1 - 1} + G_{20}(c_{11}\lambda_2 + c_{12}) r_i^{\lambda_2 - 1} + f_0 B_1 = T_0 B_0, \quad i = 1, 2, \quad (61)$$

where

$$B_1 = \begin{cases} c_{13} + (c_{23} - c_{13})(c_{11} + c_{12})/(c_{11} - c_{22}) & \text{for } c_{11} \neq c_{22} \\ c_{13} + (c_{23} - c_{13})/2 + (c_{23} - c_{13})(c_{11} + c_{12}) \ln r/(2c_{11}) & \text{for } c_{11} = c_{22}, \end{cases} \quad (62)$$

$$B_0 = \begin{cases} q_1 - q_2(c_{11} + c_{12})/(c_{11} - c_{22}) & \text{for } c_{11} \neq c_{22} \\ q_1 - q_2/2 - q_2(c_{11} + c_{12}) \ln r/(2c_{11}) & \text{for } c_{11} = c_{22} \end{cases} \quad (63)$$

The end boundary condition of zero resultant axial force, $P_z(t) = \int_{r_1}^{r_2} \sigma_{zz}(r, t) 2\pi r dr = 0$, gives the last set of equations that are needed to determine the unknown constants:

$$G_{10}\left(\frac{c_{31}\lambda_1 + c_{32}}{\lambda_1 + 1}\right)(r_2^{\lambda_1+1} - r_1^{\lambda_1+1}) + G_{20}E_2 + f_0E_1 = T_0E_0, \quad (64)$$

where the parameters used are described, for $c_{11} \neq c_{22}$, by

$$E_2 = \left(\frac{c_{13}\lambda_2 + c_{23}}{\lambda_2 + 1}\right)(r_2^{\lambda_2+1} - r_1^{\lambda_2+1});$$

$$E_1 = \left(\frac{c_{23}^2 - c_{13}^2}{c_{11} - c_{22}} + c_{33}\right)\frac{(r_2^2 - r_1^2)}{2}, \quad (65)$$

$$E_0 = \left(q_{\alpha 3} - q_2\frac{c_{13} + c_{23}}{c_{11} - c_{22}}\right)\frac{(r_2^2 - r_1^2)}{2}, \quad (66)$$

and, for $c_{11} = c_{22}$,

$$E_2 = (c_{13}\lambda_2 + c_{23}) \ln (r_2/r_1), \quad (67)$$

$$E_1 = \left(c_{33} + c_{31}\frac{c_{23} - c_{13}}{2c_{11}} - \frac{c_{23}^2 - c_{13}^2}{4c_{11}}\right)\frac{(r_2^2 - r_1^2)}{2} + \frac{c_{23}^2 - c_{13}^2}{4c_{11}}(r_2^2 \ln r_2 - r_1^2 \ln r_1), \quad (68)$$

and

$$E_0 = \left(q_{\alpha 3} - q_2\frac{c_{13}}{2c_{11}}\right)\frac{(r_2^2 - r_1^2)}{2} - (c_{31} + c_{32})\frac{q_2}{4c_{11}} \times \left[(r_2^2 \ln r_2 - r_1^2 \ln r_1) - \frac{(r_2^2 - r_1^2)}{2}\right]. \quad (69)$$

The boundary conditions for the time dependent terms in the sets of algebraic Eqs. (61) and (64) have already been satisfied by (22) and (23). Therefore there is no need for additional equations to determine the unknown constants.

Results and Discussion

In order to examine the present solution's validity, a numerical example was employed to analyze the elastodynamic thermal shock stresses propagating through the wall in the form of a stress wave. Before presenting results, it should be mentioned that the definition in the form of a series expansion for the Bessel functions cannot be used for large arguments. For large arguments, the Hankel asymptotic expansions of the Bessel functions should be used for the eigenvalues, eigenfunctions, and the evaluation of Hankel transforms as described in the Appendix A.

Table 1 The first ten roots of the transcendental Eq. (31) and the values of the arguments* at the boundaries

i	ξ_i	$r_1 \times \xi_i$	$r_2 \times \xi_i$
1	25.30	1.265	2.530
2	68.56	3.428	6.856
3	128.4	6.422	12.84
4	190.3	9.517	19.03
5	252.7	12.64	25.27
6	315.3	15.76	31.53
7	377.9	18.90	37.79
8	440.6	22.03	44.06
9	503.3	25.17	50.33
10	566.1	28.30	56.61

* In computing the Bessel functions, the Hankel asymptotic expansions are used above the value of 18.0 (large arguments region).

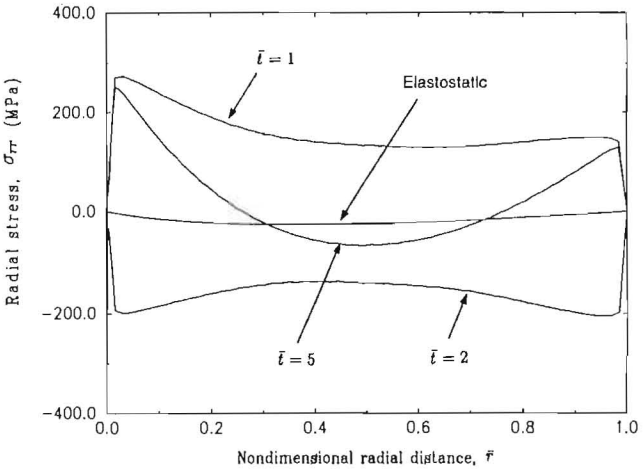

Fig. 1 The distribution of radial stress, σ_{rr}, from the elastodynamic solution at different times versus the nondimensional radial distance, $\bar{r} = (r - r_1)/(r_2 - r_1)$. Also the elastostatic solution is shown.

As an illustrative example, the distributions and histories of thermal shock stresses in the wall are determined for a glass/epoxy circular cylinder of inner radius $r_1 = 50$ mm and outer radius $r_2 = 100$ mm. It is supposed to be made, by filament winding, with the fibers oriented around the circumference of cylinder. The moduli in GN/m^2 and Poisson's ratios for the material are listed in the following, where 1 denotes the radial (r), 2 the circumferential (θ), and 3 the axial (z) direction:

$$E_1 = 13.7, \quad E_2 = 55.9, \quad E_3 = 13.7, \quad G_{12} = 5.6, \quad G_{23} = 5.6$$
$$G_{31} = 4.9, \quad \nu_{12} = 0.068, \quad \nu_{23} = 0.277, \quad \nu_{31} = 0.4.$$

The thermal expansion coefficients are $\alpha_r = 40 \times 10^{-6}$/°C, $\alpha_\theta = 10 \times 10^{-6}$/°C, and $\alpha_z = 40 \times 10^{-6}$/°C. The loading temperature of $T(r, t)$, causing thermal shock at the surface, is applied at $t = 0^+$ over the entire thickness of the hollow cylinder, and it is assumed that the applied temperature is kept constant thereafter. This type of thermal loading, causing the response of strong dynamic thermal stresses on the cylinder, can be developed by a strong chemical reaction, an absorption of infrared radiation, or an electromagnetic radiant energy from pulses.

For the eigenfunction series sum of the elastodynamic solution, roots of the transcendental Eq. (31) are needed. The first ten roots are shown in the Table 1 with the values of the arguments at both boundaries. Numerical finite Hankel transformations for arbitrary functions were carried out by using the Romberg's integration algorithm.

In order to show the results, the following nondimensional quantities are used: for radial distance (through the thickness), $\bar{r} = (r - r_1)/(r_2 - r_1)$, and for time, $\bar{t} = \bar{c}t/(r_2 - r_1)$, where $\bar{t}$ would physically represent the number of trips required by the stress wave in going through the thickness. The distribution of radial dynamic thermal stress is presented at each nondimensional time $\bar{t} = 1$, 2, and 5 in Fig. 1. Since the speed of wave $\bar{c}$ is calculated as 3,169 m/sec, the nondimensional time $\bar{t} = 1$ indicates 1.577×10^{-5} sec. The radial stress wave is initiated at the inside and outside boundaries simultaneously, propagates outward from the inside boundary and inward from the external boundary through the wall and reflects in the opposite direction towards the boundaries. Subsequently, this reflected wave is also reversed again at the boundaries. The tension in the first phase of travel is reversed into compression by the reflection

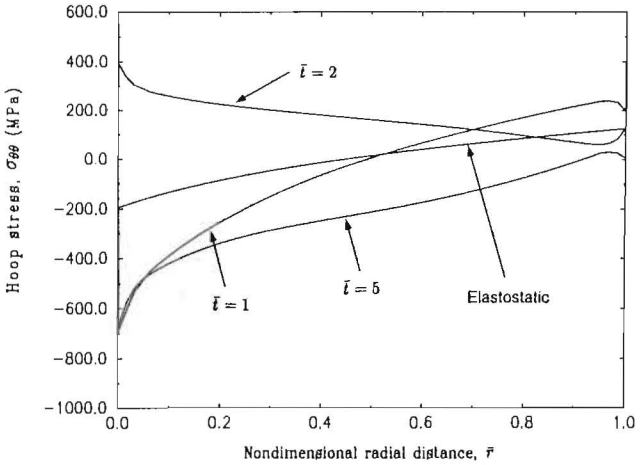

Fig. 2 The distribution of hoop stress, $\sigma_{\theta\theta}$, at different times versus the nondimensional radial distance, $\bar{r} = (r - r_1)/(r_2 - r_1)$

of waves, as shown in Figs. 4(*a*, *b*), and a dramatic change of radial stress through the thickness is observed. This effect is reduced with time. The first maximum peak radial stress is obtained at $\bar{r} = 0.5$ when $\bar{t} = 5.5$. As expected, the magnitude of dynamic radial stress is much higher than that in the static case.

The largest change of stresses through the shell thickness is observed in the circumferential direction during the first travel of the wave, as shown in Fig. 2. The magnitude of the hoop stresses near the boundaries increases with continuing wave propagation. The hoop stress near the midpoint in the wall is lower than that near the boundaries. The maximum dynamic thermal stress on a circumferentially wound orthotropic cylindrical shell occurs in the first travel in the circumferential direction at the inner boundary. This observation for an orthotropic cylindrical shell is still true as in the isotropic case which was observed in Wang (1995). It should be noted that the cylinder is most resistant in this direction, since it is circumferentially filament wound and the material strength in the fiber direction is usually the largest. Therefore, this dominant material characteristic affects to a large extent the elastodynamic response of the cylindrical shell structure. Of course, in addition to the stiffness and strength in the fiber direction, the thermal expansion coefficients are also important factors in determining the thermoelastic behavior of an orthotropic thick cylindrical shell. The axial stress in Fig. 3 is not significant in comparison with the radial and hoop stresses. Actually, the behavior of axial stress is similar to that of the radial stress.

The time history of the radial stress is shown at $\bar{r} = 0.1$ in Fig. 4(*a*) and $\bar{r} = 0.5$ in Fig. 4(*b*) (notice the high-frequency oscillations). The peaks of radial stress appear whenever the stress wave reaches the corresponding locations. The steep change of magnitude of radial stress is seen near each observing location. In Fig. 5, it is clear that the hoop stress at $\bar{r} = 0.5$ experiences a smaller change than that at $\bar{r} = 0$ and $\bar{r} = 1$. This phenomenon can be observed in Fig. 2, as well. The maximum stress is observed at $\bar{t} = 5$ and 10 in the circumferential direction. The time history of axial stress is given in Fig. 6. The axial stress also has sharp peaks at $\bar{r} = 0.5$ when a stress wave arrives at that location. This characteristic of axial stress isn't seen in Fig. 3 because the time selected corresponds to the absence of points when the waves arrive.

To compare the effects of stresses for an orthotropic thick cylindrical shell to that of the isotropic case, the distribution of radial stress at $\bar{t} = 1$, 2, 5, and 10 in Fig. 7 is carried out after selecting for the orthotropic moduli, in GN/m^2 and the other material constants:

$$E = E_i = 55.9, \quad \nu = \nu_{ij} = 0.277,$$

$$\alpha = \alpha_i = 10 \times 10^{-6}/°\text{C}, \quad i = 1, 2, 3,$$

i.e., the constants of the orthotropic shell in the circumferential direction. It is seen that a large amount of stress variation

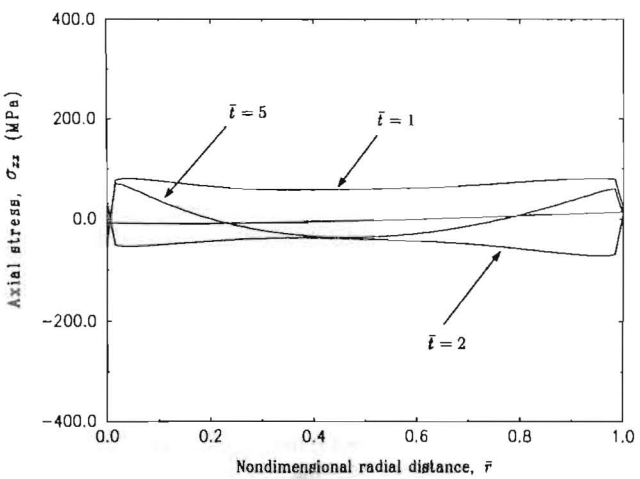

Fig. 3 The distribution of axial stress, σ_{zz}, at different times versus the nondimensional radial distance, $\bar{r}$

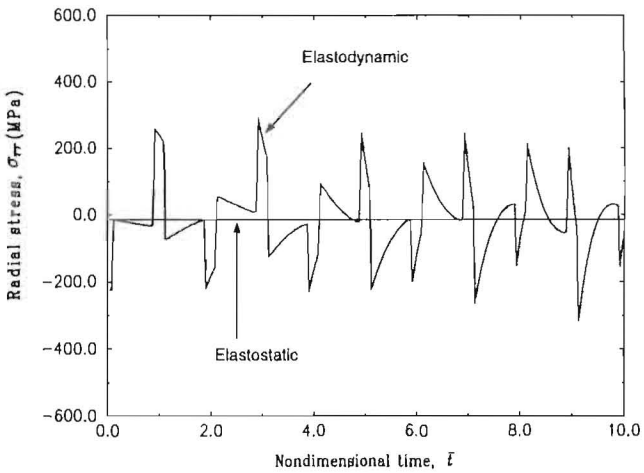

Fig. 4(*a*) The time history of radial stress, σ_{rr}, versus the nondimensional time $\bar{t} = \bar{c}t/(r_2 - r_1)$, at $\bar{r} = 0.1$

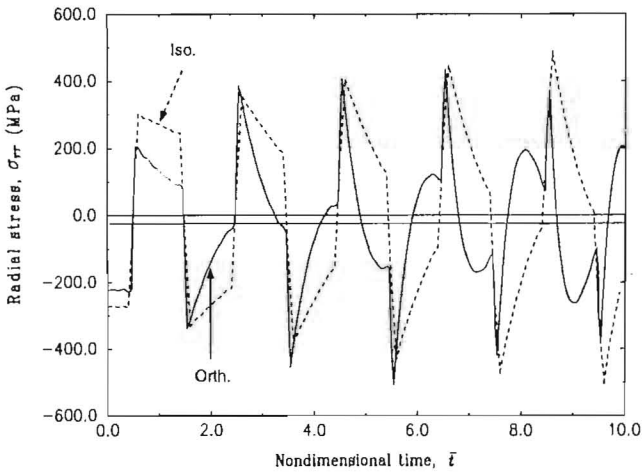

Fig. 4(*b*) The time history of radial stress, σ_{rr}, versus the nondimensional time $\bar{t} = \bar{c}t/(r_2 - r_1)$, at $\bar{r} = 0.5$

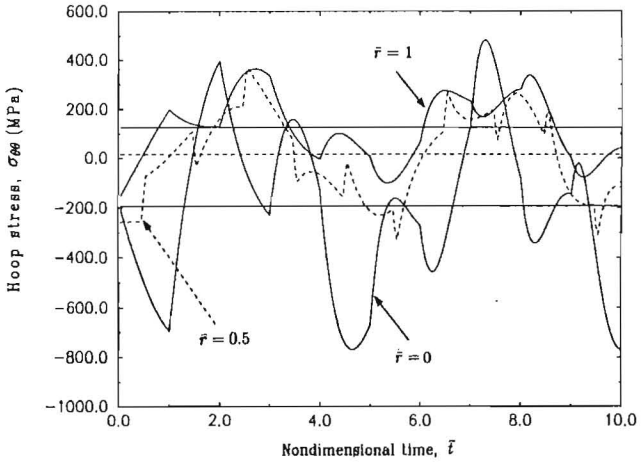

Fig. 5 The time history of hoop stress, $\sigma_{\theta\theta}$, versus the nondimensional time, $\bar{t} = \bar{c}t/(r_2 - r_1)$, at different positions through the shell thickness

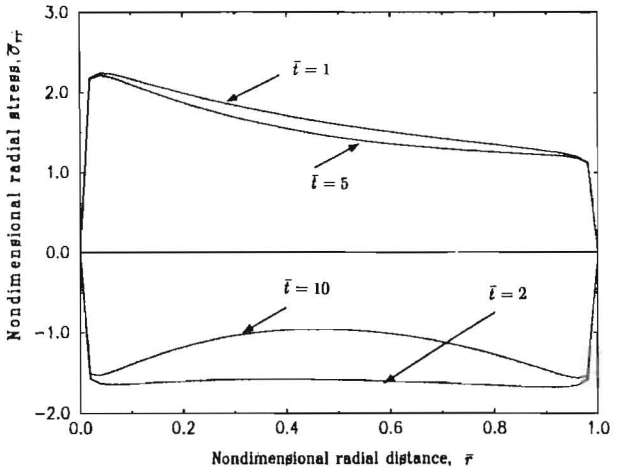

Fig. 7 The distribution of radial stress, $\overline{\sigma_{rr}}$, at $\bar{t}$ = 1, 2, 5, and 10

through the wall exists in an orthotropic cylindrical shell (Fig. 1). Thus, the peaks near the boundaries are much higher than these in other locations. The magnitude of radial stress in an orthotropic cylindrical shell drops near the center and has an oscillatory behavior attributed to the direct contribution of static stress and the orthotropic characteristics of elastic constants and thermal expansion coefficients. This effect can not be seen in the isotropic case. The oscillating behavior would come even at large time values due to the interference of the stress waves. The main difference between the two material systems appears in Figs. 1 and 7. The wavefront in an orthotropic shell is more rapidly interfered than that in an isotropic shell, as shown in Figs. 4(a, b). Also, Fig. 7, where the normalized radial stress is defined as $\bar{\sigma}_{rr} = \sigma_{rr}/E\alpha T$, and its plot shows almost the same shape and magnitude with the result given by Wang (1995). In Fig. 9, a comparison of the time history of the radial stress at $\bar{r} = 0.5$, is shown. One of the differences between the two studies is that a plane-strain condition, $\epsilon_{zz} = 0$ was imposed in that study, unlike the present one. The differences between the two results, however, most likely should be due to the differences in the calculation points. The peak values of Wang's (1995) solution are on the present study's curves but the wave patterns are different after the first trip. This seems to be due to the fact that the plot in Wang (1995) was made from data at time values not closely enough, therefore missing the peaks values of the stress wave. This comparison also makes an important point: that the time scale of calculations of data points should be carefully examined to make sure the entire response of the stress wave and especially the peaks are captured.

Finally, one more result is presented regarding the phenomena of initial wave propagation. Figure 8 for an isotropic shell can help the understanding of the early phase of stress distribution due to wave occurrence and propagation. Since the thermal loading is applied to the entire hollow cylinder instantaneously, the stress disturbance is simultaneously generated all over the wall. In the vicinity of the boundary, the radial stress feels the strong discontinuity (wavefront) right after the loading. Each wavefront moves inward and the waves meet at the center location and cause a stress reversion and sudden jump in magnitude, as shown in Figs. 4(a, b). After that, the wavefronts proceed to the boundaries continuously. When the wavefronts reach the boundaries, they are reflected into the opposite direction as mentioned earlier.

In this study, it should be mentioned that the coupling effects between the thermal and mechanical energy in the system are neglected. This means that the uncoupled linear dynamic thermoelasticity problem was handled. Since the coupling effects always exist in the physical system under thermal environments, the coupled dynamic thermoelasticity is more realistic but too difficult and complex or sometimes impossible to obtain the closed-form solution. The uncoupled dynamic thermoelasticity problem, which was treated here, is, however, still valuable and

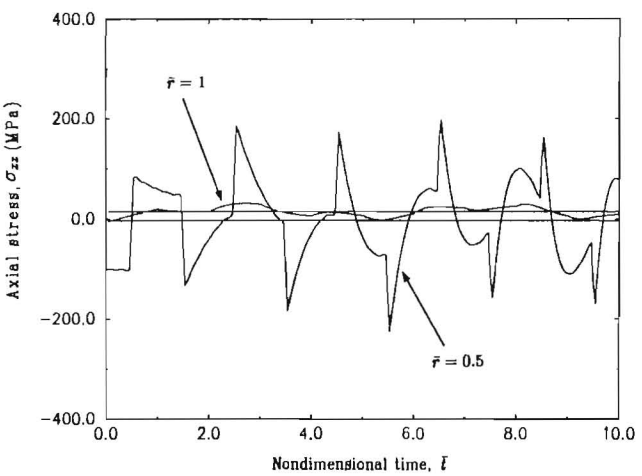

Fig. 6 The time history of axial stress, σ_{zz}, versus the nondimensional time, $\bar{t} = \bar{c}t/(r_2 - r_1)$, at $\bar{r}$ = 0.5 and 1.0

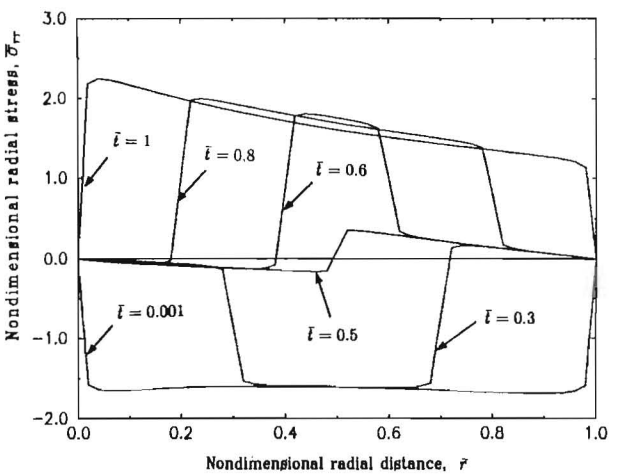

Fig. 8 The propagation of the radial stress wave, $\overline{\sigma_{rr}}$, versus $\bar{r}$ at different times

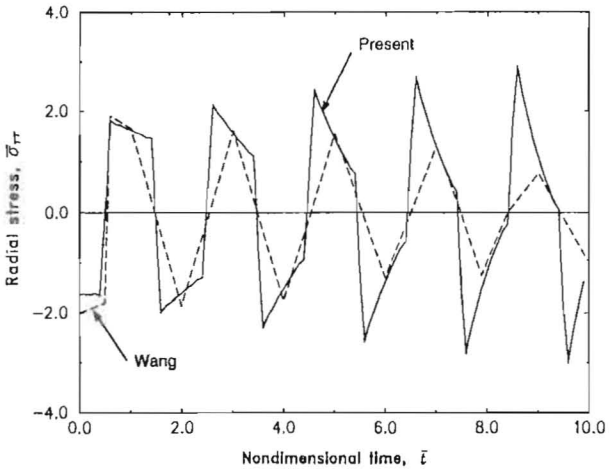

Fig. 9 Comparison of $\bar{\sigma}_{rr}$ at $\bar{r} = 0.5$, for the isotropic case, with the results of Wang (1995)

can provide a large amount of useful information on the thermal shock effects. Finally, the shell axisymmetry concept, in conjunction with the radial dependence of the thermal field, limit the applicability of the results to essentially infinitely long shells.

Summary

This work presents a method to analyze the uncoupled dynamic thermoelastic stress problem in an orthotropic thick cylindrical shell. In implementing the method, the linear dynamic thermoelasticity equations are used with the appropriate boundary and initial conditions, and the elastodynamic problem is solved by using the finite Hankel transform in the spatial variable and the Laplace transform in the time variable. In this paper, the temperature distribution was considered as the step function applied to the entire surface of the hollow cylinder. It is shown that a closed-form solution can be obtained for the thermal shock stresses in an orthotropic thick cylindrical shell. As seen in the results, a thermal stress wave occurs due to the thermal shock loading, and this plays an important role on the significant amount of dynamic thermal stresses generated through the wall. Important differences between an isotropic and orthotropic cylindrical shell exist, namely rapid variations of radial stresses in the orthotropic case, which are attributed to the orthotropy of the mechanical and thermal properties.

Acknowledgment

The financial support of the Office of Naval Research, Ship Structures and Systems, S&T Division, Grant N00014-91-J-1892, and the interest and encouragement of the Grant Monitor, Dr. Y. D. S. Rajapakse, are both gratefully acknowledged.

References

Abramowitz, M., and Stegun, I. A., 1972, *Handbook of Mathematical Functions with Formulas, Graphs and Mathematical Tables,* Dover, New York.

Achenbach, J. D., 1973, *Wave Propagation in Elastic Solids,* North-Holland, Amsterdam.

Birman, V., 1990, "Thermal Dynamic Problems of Reinforced Composite Cylinders," ASME JOURNAL OF APPLIED MECHANICS, Vol. 57, pp. 941–947.

Churchill, R. V., 1972, *Operational Mathematics,* 3rd. ed., McGraw-Hill, New York.

Cinelli, G., 1965, "An Extension of the Finite Hankel Transform and Applications," *International Journal of Engineering Science,* Vol. 3, pp. 539–559.

Cinelli, G., 1966, "Dynamic Vibrations and Stresses in Elastic Cylinders and Spheres," ASME JOURNAL OF APPLIED MECHANICS, Vol. 33, pp. 825–830.

Doxee, Jr., L. E., and Springer, G. S., 1989, "Hygrothermal Stresses and Strains in Axisymmetric Composite Shells," *Computers and Structures,* Vol. 32, No. 2, pp. 395–407.

Eringen, A. C., and Suhubi, E. S., 1975, *Elastodynamics* (Vol. II, Linear Theory), Academic Press, New York.

Graff, K. F., 1975, *Wave Motion in Elastic Solids,* Ohio State University Press, Columbus, OH.

Hata, T., 1991, "Thermal Shock in a Hollow Sphere Caused by Rapid Uniform Heating," ASME JOURNAL OF APPLIED MECHANICS, Vol. 58, pp. 64–69.

Hyer, M. W., and Cooper, D. E., 1986, "Stresses and Deformations in Composite Tubes due to a Circumferential Temperature Gradient," ASME JOURNAL OF APPLIED MECHANICS, Vol. 53, pp. 757–764.

Kardomateas, G. A., 1989, "Transient Thermal Stresses in Cylindrically Orthotropic Composite Tubes," ASME JOURNAL OF APPLIED MECHANICS, Vol. 56, pp. 411–417; also Errata, Ibid, 1991, Vol. 58, p. 909.

Kardomateas, G. A., 1990, "The Initial Phase of Transient Thermal Stresses due to General Boundary Thermal Loads in Orthotropic Hollow Cylinders," ASME JOURNAL OF APPLIED MECHANICS, Vol. 57, pp. 719–724; also Errata, Ibid, 1991, Vol. 58, p. 909.

Lebedev, N. N., 1972, *Special Functions and their Applications,* Dover, New York.

Lekhinitskii, S. G., 1981, *Theory of Elasticity of an Anisotropic Body,* Mir Publishers, Moscow.

McLachan, N. W., 1934, *Bessel Functions for Engineers,* Oxford, London.

McQuillen, E. J., and Brull, M. A., 1970, "Dynamic Thermoelastic Response of Cylindrical Shells," ASME JOURNAL OF APPLIED MECHANICS, Vol. 37, pp. 661–670.

Sciuva, M. D., and Carrera, E., 1992, "Elastodynamic Behavior of Relatively Thick, Symmetrically Laminated, Anisotropic Circular Cylindrical Shells," ASME JOURNAL OF APPLIED MECHANICS, Vol. 59, pp. 222–224.

Sneddon, I. N., 1995, *Fourier Transforms,* Dover, New York (original printed in 1951).

Sternberg, E., and Chakravorty, J. G., 1959, "Thermal Shock in an Elastic Body with a Spherical Cavity," *Quart. Applied Mathematics,* Vol. 17, pp. 205–218.

Tsui T., and Kraus H., 1965, "Thermal Stress Wave Propagation in Hollow Elastic Spheres," *Journal of the Acoustical Society of America,* Vol. 37, pp. 730–737.

Wang, X., and Gong, X. N., 1992, "An Elastodynamic Solution for Multilayered Cylinders," *International Journal of Engineering Science,* Vol. 30, No. 1, pp. 25–33.

Wang, X., 1995, "Thermal Shock in a Hollow Cylinder Caused by Rapid Arbitrary Heating," *Journal of Sound and Vibration,* Vol. 183, No. 5, pp. 899–906.

Wang, X., 1993, "Stress Wave Propagation in a Two Layered Cylinder with Initial Interface Pressure," *International Journal of Solids and Structures,* Vol. 30, No. 12, pp. 1693–1700.

Zaker, T. A., 1969, "Dynamic Thermal Shock in a Hollow Sphere," *Quart. Applied Mathematics,* Vol. 26, pp. 503–518.

APPENDIX A

The definition of Bessel functions of the first kind of order υ is for small arguments:

$$J_\nu(z) = \sum_{m=0}^{\infty} \frac{(-1)^m (1/2)^{2m+\nu}}{m!\Gamma(m+\nu+1)} z^{2m+\nu}, \quad m = 1, 2, 3, \ldots, \quad (A1)$$

$$J_{-\nu}(z) = \sum_{m=0}^{\infty} \frac{(-1)^m (1/2)^{2m-\nu}}{m!\Gamma(m-\nu+1)} z^{2m-\nu}, \quad m = 1, 2, 3, \ldots. \quad (A2)$$

The Hankel's asymptotic expansions for large arguments, when ν is fixed and $|z|$ goes to infinity, are described in the following:

$$J_\nu(z) = \sqrt{2/(\pi z)}\,[P(\nu, z)\cos\chi - Q(\nu, z)\sin\chi], \quad (A3)$$

$$Y_\nu(z) = \sqrt{2/(\pi z)}\,[P(\nu, z)\sin\chi + Q(\nu, z)\cos\chi], \quad (A4)$$

where the parameter $\chi = z - (\frac{1}{2}\nu + \frac{1}{4})\pi$, and, with $4\nu^2$ denoted by μ, P, and Q are defined by

$$P(\nu, z) = \sum_{k=0}^{\infty} (-1)^k \frac{(\nu, 2k)}{(2z)^{2k}} = 1 - \frac{(\nu-1)(\nu-9)}{2!(8z)^2} + \ldots, \quad (A5)$$

$$Q(\nu, z) = \sum_{k=0}^{\infty} (-1)^k \frac{(\nu, 2k+1)}{(2z)^{2k+1}}$$

$$= \frac{(\nu-1)}{(8z)} - \frac{(\nu-1)(\nu-9)(\nu-25)}{3!(8z)^3} + \ldots . \quad (A6)$$

APPENDIX B

The finite Hankel transformations of arbitrary functions can be evaluated analytically by using the series expansion form of the Bessel functions for small arguments. By the recurrence formula, the finite Hankel transforms for r^{ν} and $r^{-\nu}$ can be expressed as

$$I_1(\xi_i) = \int_{r_1}^{r_2} r^{\nu+1} D_\nu(\xi_i r) dr = J_{-a}\left[\frac{r^{\nu+1}}{\xi_i} J_{\nu+1}(\xi_i r)\right]_{r_1}^{r_2}$$

$$- J_a\left[-\frac{r^{\nu+1}}{\xi_i} J_{-\nu-1}(\xi_i r)\right]_{r_1}^{r_2}, \quad (B1)$$

$$I_2(\xi_i) = \int_{r_1}^{r_2} r^{-\nu+1} D_\nu(\xi_i r) dr = J_{-a}\left[-\frac{r^{-\nu+1}}{\xi_i} J_{\nu-1}(\xi_i r)\right]_{r_1}^{r_2}$$

$$- J_a\left[\frac{r^{-\nu+1}}{\xi_i} J_{-\nu+1}(\xi_i r)\right]_{r_1}^{r_2}. \quad (B2)$$

For r, the finite Hankel transform is given by

$$I_3(\xi_i) = \int_{r_1}^{r_2} r^2 D_\nu(\xi_i r) dr = J_{-a}\left[\sum_{m=0}^{\infty} \frac{A_m r^{2m+\nu+3}}{2m+\nu+3}\right]_{r_1}^{r_2}$$

$$- J_a\left[\sum_{m=0}^{\infty} \frac{A_{-m} r^{2m-\nu+3}}{2m-\nu+3}\right]_{r_1}^{r_2}, \quad (B3)$$

where

$$A_m = \frac{(-1)^m (1/2)^{2m+\nu}}{m!\Gamma(m+\nu+1)}, \quad A_{-m} = \frac{(-1)^m (1/2)^{2m-\nu}}{m!\Gamma(m-\nu+1)}. \quad (B4)$$

CONTENTS (CONTINUED)

ANNOUNCEMENTS AND SPECIAL NOTICES